## RESEARCH

# Monoexponential, biexponential and diffusion kurtosis MR imaging models: quantitative biomarkers in the diagnosis of placenta accreta spectrum disorders

Tao Lu[1], Yishuang Wang[1], Aiwen Guo[1], Wei Cui[1], Yazheng Chen[1], Shaoyu Wang[2] and Guotai Wang[3*]

## Abstract

**Background:** To investigate the diagnostic value of monoexponential, biexponential, and diffusion kurtosis MR imaging (MRI) in differentiating placenta accreta spectrum (PAS) disorders.

**Methods:** A total of 65 patients with PAS disorders and 27 patients with normal placentas undergoing conventional DWI, IVIM, and DKI were retrospectively reviewed. The mean, minimum, and maximum parameters including the apparent diffusion coefficient (ADC) and exponential ADC (eADC) from standard DWI, diffusion kurtosis (MK), and mean diffusion coefficient (MD) from DKI and pure diffusion coefficient (D), pseudo-diffusion coefficient (D*), and perfusion fraction (f) from IVIM were measured from the volumetric analysis and compared between patients with PAS disorders and patients with normal placentas. Univariate and multivariated logistic regression analyses were used to evaluate the value of the above parameters for differentiating PAS disorders. Receiver operating characteristics (ROC) curve analyses were used to evaluate the diagnostic efficiency of different diffusion parameters for predicting PAS disorders.

**Results:** Multivariate analysis demonstrated that only D mean and D max differed significantly among all the studied parameters for differentiating PAS disorders when comparisons between accreta lesions in patients with PAS (AP) and whole placentas in patients with normal placentas (WP-normal) were performed (all $p < 0.05$). For discriminating PAS disorders, a combined use of these two parameters yielded an AUC of 0.93 with sensitivity, specificity, and accuracy of 83.08, 88.89, and 83.70%, respectively.

**Conclusion:** The diagnostic performance of the parameters from accreta lesions was better than that of the whole placenta. D mean and D max were associated with PAS disorders.

**Keywords:** PAS disorders, Diffusion-weighted MRI, Intravoxel incoherent motion, Diffusion kurtosis imaging

## Key points

1. Volumetric analysis of different DWI models can lend strong support to quantitative evaluation of the heterogeneity, cellularity, and microvascular perfusion of the PAS disorders.
2. PAS disorders can be differentiated effectively with the combined use of the different DWI parameters.

*Correspondence: guotai.wang@uestc.edu.cn
[3] School of Mechanical and Electrical Engineering, University of Electronic Science and Technology of China, 2006 Xiyuan Avenue, West Hi-tech Zone, Chengdu 611731, China
Full list of author information is available at the end of the article

Lu *et al. BMC Pregnancy and Childbirth*     (2022) 22:349

Page 2 of 12

# Background

Placenta accreta spectrum (PAS) disorders refer to an abnormal condition where the placental chorionic villi adhere to or invade the myometrium, entering into a place with deficient decidual formation [1, 2]. The incidence of PAS kept rising from 1 in 30,000 to 1 in 300 gravidas over the past four decades [3, 4], mainly as cesarean deliveries increasing [5]. The major problem of PAS resulting from unsuccessful clean placental detachment after delivery is massive obstetric hemorrhage accompanied by secondary complications including coagulopathy, multisystem organ failure, hysterectomy, and even death [6–10].

Ultrasonography remains the first-line modality for detecting PAS disorders but is limited in assessing the posterior placenta and by patients' body habitus. MRI has been increasingly a complementary modality for the prenatal diagnosis of PAS disorders in recent years. However, according to a recent systematic review, the sensitivity and specificity of MRI in diagnosing PAS varied widely between 75 and 100% and 65–100%, respectively [11]. The discrimination of typical MRI features related to PAS disorders is proposed to require expertise and doctors' experience. The interobserver agreement in identifying the presence and depth of placental invasion was excellent, but the interrater agreement in ascertaining the topography of the invasion was lower even in hands of experienced examiners [12].

Meanwhile, quantification of placental function and identification of mothers at high risk are both important in today's clinical practice. Conventional DWI is a monoexponential Gaussian model, evaluating the diffusion restriction of water molecules in tissue using apparent diffusion coefficient (ADC). eADC (exponential apparent diffusion coefficient) is another parameter of DWI used in recent years with eADC images eliminating the T2 shine through effect. However, it is considered that the diffusion of water molecules in biological tissue is much more complicated and restricted by microstructures, such as cell membranes and organelles, which follow a non-Gaussian behavior [13]. Diffusion kurtosis imaging (DKI), first proposed by Jensen et al. [14, 15], allows the accurate estimation of water diffusivity in biological tissue and quantification of tissue heterogeneity and cellularity with higher b values [13, 14]. However, the measured diffusion signals in living tissue are also influenced by the perfusion of blood micro-vascularization at low b values besides the motion of water molecules [16, 17]. IVIM, first proposed by Le Bihan et al. [16], is a biexponential model that separates microvascular perfusion from water diffusivity within the tissue [16, 17]. Some researchers have investigated the feasibility of IVIM in pregnancies complicated by placental dysfunction due to vascular malperfusion [18], placenta accreta [19–21], preeclampsia [22], growth-restricted pregnancy [23], and normal pregnancies [24–26].

Theoretically, PAS placenta might show vascularity and blood flow different from the normal placenta and these changes can be detected by different DWI models, and thus we here attempted to determine whether these DWI models can be used to predict PAS. Therefore, this study primarily aimed to apply these promising advanced DWI models besides the conventional DWI model to evaluate the placental function in patients with PAS disorders and, secondly, evaluate whether the diagnostic parameters derived from different DWI models could be served as quantitative biomarkers for diagnosing PAS disorders.

# Materials and methods

This study was approved by the institutional review board (IRB) and obtained written informed consent from each woman participants. During November 2018 and March 2021, a total of 172 patients were initially scanned with a DWI sequence during the study period. The inclusion criteria were (1) suspected PAS disorders based on clinical risk factors or previous ultrasound (US) results, (2) singleton pregnancy, (3) fetal development coinciding with gestational age. Patients were excluded for the following reasons (1) chronic hypertension, pre-existing renal disease, and diabetes mellitus, (2) inadequate surgical records, (3) suspected placental insufficiency, (4) severe artifacts on MRI images. Placenta previa without PAS was considered normal in this study. Finally, a total of 92 patients (mean age $31.67 \pm 4.58$ years, range 22–45 years) were enrolled (Fig. 1). The average gestational age was 32 weeks (range 16–38 weeks).

## MRI protocols

MRI examinations were performed on a 1.5 T MR scanner (Aera, Siemens Healthineers, Erlangen, Germany) using a 16-channel body matrix coil. Conventional MR sequences including HASTE, True-FISP, and T1WI were scanned, then DWI was performed by using a single-shot echo-planar imaging (EPI) sequence with a pair of rectangular diffusion gradient pulses along all three orthogonal axes. The imaging parameters were as follows: TR/TE = 5200/83 ms, number of averages = 2, acquisition matrix = $192 \times 120$, field of view (FOV) = 390 mm, slice thickness = 5 mm, intersection gap = 5 mm, and parallel imaging acceleration factor = 2. Eleven different b values ranging from 0 to 1600 s/mm$^2$ (b = 0, 50, 100, 150, 200, 400, 600, 800, 1000, 1200, and 1600 s/mm$^2$) were applied. The total scan time for the DWI sequence was 7 min 29 s.

Lu *et al. BMC Pregnancy and Childbirth*    (2022) 22:349

Page 3 of 12



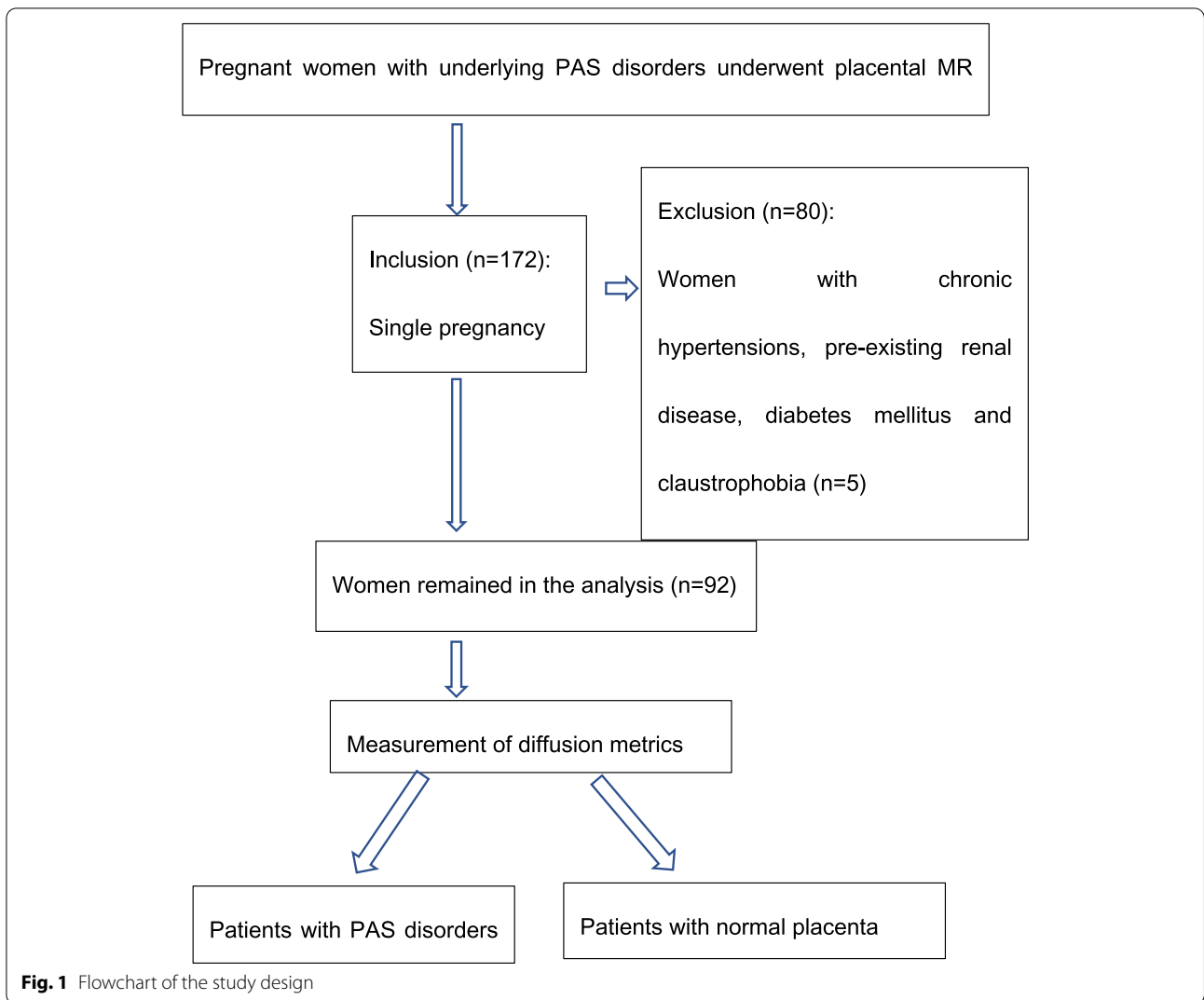**Fig. 1** Flowchart of the study design

**Image processing and analysis**

ROI delineation and calculation of the DWI, DKI, IVIM parameters were performed using research software IMA-genGINE (Vusion Tech) [27]. For standard monoexponential DWI analysis, b values of 0 and 1000 s/mm² were used to fit the following equation:

$$Sb/S0 = \exp(-b \times ADC)$$

where Sb and S0 are the signal intensities in the diffusion gradient factors of b and 0, respectively. ADC can be calculated by fitting the signal to this model, and the exponential ADC (eADC) is calculated through the formula:

$$Sb/S0 = \text{Exponential ADC} = \exp[-(b \times ADC)]$$

For DKI analysis, 6 b-values (b = 0, 400, 800, 1000, 1200, and 1600 s/mm²) are used to perform the model fitting the following equation [28, 29]:

$$Sb/S0 = \exp(-b \times MD + b^2 \cdot MD^2 \times MK/6)$$

where Sb and S0 are the signal intensities acquired with the diffusion gradient factors of b and 0, respectively. MD is the mean diffusivity representing the corrected ADC, MK is the diffusion kurtosis.

For IVIM analysis, 8 b-values (b = 0, 50, 100, 150, 200, 400, 600, 800 s/mm²) were used to perform the model fitting the following equation [30, 31]:

$$Sb/S0 = (1 - f)\exp(-b \times D) + f\exp[-b \times (D + D^*)]$$

where Sb and S0 are the signal intensities in the diffusion gradient factors of b and 0, respectively. IVIM parameters, including D, D*, and f, can be derived from

Lu *et al. BMC Pregnancy and Childbirth*    (2022) 22:349

Page 4 of 12

the model. f is the perfusion fraction, D is the diffusion coefficient, and D* is the pseudo-diffusion coefficient.

All ROIs were drawn independently by two radiologists with 5 and 8 years of experience in obstetric imaging, respectively. All patients' whole placenta ROIs were drawn on each consecutive DWI with b = 0 s/mm² covering the whole placenta, referring to conventional T2WI. PAS-ROIs were drawn covering the accreta lesions. The ROI size was slightly smaller than the visible margin of the placenta to avoid partial volume effect and was then automatically copied to all diffusion parameter maps. The mean, minimum, and maximum ADC (ADC mean, ADC min, and ADC max), eADC (eADC mean, eADC min, and eADC max), MD (MD mean, MD min, and MD max), MK (MK mean, MK min, and MK max), D (D mean, D min, and D max), D* (D* mean, D* min, and D* max), and f (f mean, f min, and f max) values were automatically calculated, and the diffusion parameter maps were also automatically produced. The measurements made by the first reader were used to evaluate the intra-reader reproducibility with a minimum washout period of at least 1 month, while the measurements made by two readers were used to evaluate the inter-reader reproducibility and were averaged for statistical analysis.

### Reference standard

The diagnosis of PAS disorders was made intraoperatively. Placenta percreta was diagnosed when the placental tissue invaded the uterine serosa and surrounding organs, including the broad ligament, vaginal wall, and bladder visually [32]. During the 3rd stage of labor, placenta increta was diagnosed when the placenta did not separate after 20 min despite active management, resulting in a difficult manual piecemeal removal of the placenta and heavy bleeding from the implantation site [32]. Placenta creta was diagnosed when the placenta firmly adhered to the endometrium with uncontrollable bleeding at the time of removal [32]. Pathological examination was performed from uterine specimens in hysterectomy cases or from placental tissue in the invasive site.

### Statistical analysis

The heterogeneity and diffusion parameters of the placenta changed with the increase of gestational weeks. All the parameters were corrected using the following equation to remove changes induced by gestational age [33]:

$$y_{corrected} = y - \beta X_{age} = y - \begin{pmatrix} \beta_0 \\ \beta_c \end{pmatrix} X_{age}$$

Where $y_{corrected}$ is the value after correction, $y$ is the original value, $X_{age}$ is the gestational week vector, and $\beta_0$ and $\beta_c$ are the constant and the linear regression coefficient in linear fitting, respectively.

A two-sample independent t-test was used to compare the difference in the DWI parameters of the whole placenta between patients with PAS disorders and patients with normal placenta, and also was used to compare the difference between accreta lesions in patients with PAS disorders and patients with normal placentas. Receiver operating characteristics (ROC) analyses were performed to evaluate the diagnostic performance of significant parameters from measuring the whole placenta and accreta lesions in patients with PAS disorders, respectively, in predicting PAS disorders. Youden index and corresponding sensitivity, specificity, positive and negative likelihood ratio were calculated. Z test was used to compare AUCs. The significant DWI parameters showing the highest Youden index were included for the differentiation. Univariate and multivariated logistic regression analyses were used to identify independent risk factors of PAS disorders. The inter-reader and intra-reader reproducibility for parameter measurements was evaluated using the intraclass correlation coefficient (ICC) with 95% confidence intervals (CI). *P* values < 0.05 were considered statistically significant. All analyses were performed on a Win10 desktop with Python 3.6, scipy 1.5.2 and sklearn 0.24.1 [34].

### Results

Table 1 presents the maternal characteristics of the study participants. Sixty-five patients (70.65%) with PAS disorders including 12 (13.04%) patients with placenta creta, 46(50%) patients with placenta increta, 7(7.61%) patients with placenta percreta, and 27(29.35%) patients with normal placentas remained in the analysis. Of the 27 patients without PAS disorders,16 patients had vaginal delivery and 11 patients had cesarean delivery. Of the 65 patients with PAS disorders, 3 patients had hysterectomy, 57 patients had forcible separation and hemostasis, 5 patients had forcible separation without hemostasis.

Patients with PAS disorders were older than those with normal placentas (*p* = 0.002), and more patients with PAS disorders were over 35 years old (*p* = 0.026). Patients with PAS disorders also delivered earlier, had more CDs, previous uterine dilations and curettages, and placenta previa (*p* = 0.000 respectively).

Intra- and inter-observer agreement varied from 0.839 to 0.979 (Table 2). Overall, the Intra- and inter-observer agreements were excellent for the volumetric analysis of the placenta.

Volumetric analysis of whole placenta comparisons between patients with normal placentas (WP-normal) and patients with PAS disorders (WP-PAS) was performed, showing that MD mean, MD max, f mean, D mean, and D* mean were significantly higher while MK mean, MD min and D max were significantly lower

Lu *et al. BMC Pregnancy and Childbirth*        (2022) 22:349

Page 5 of 12

**Table 1** Maternal characteristics in the study groups

|  | Patients with normal placenta | Patients with PAS disorders | P value |
|---|---|---|---|
| **Number** | 27 | 65 | |
| **Age (years)** | 29.37 ± 4.34 | 32.63 ± 4.36 | 0.026 |
| Less than 35 | 24 (88.89%) | 43 (66.15%) | |
| 35 or older | 3 (11.11%) | 22 (33.85%) | |
| **Gestational age At examination (weeks)** | 32 (6) | 32 (5) | 0.611 |
| **Gestational age At the time of delivery (weeks)** | 38 (2) | 36 (3) | 0.000 |
| **Number of Previous caesarean Section** | | | |
| 0 | 13 (48.15%) | 7 (10.77%) | |
| 1 | 12 (44.44%) | 54 (83.08%) | |
| 2 or more | 2 (7.41%) | 4 (6.15%) | 0.000 |
| **Previous uterine Dilation and Curettage** | | | |
| No | 9 (3.33%) | 2 (3.01%) | |
| Yes | 18 (66.67%) | 63 (96.92%) | 0.000 |
| **Placenta previa** | | | 0.000 |
| **No** | 16 (59.26%) | 4 (6.15%) | |
| **Yes** | 11 (40.74%) | 61 (93.85%) | |
| **Placental position** | | | 0.052 |
| **Anterior** | 12 (44.44%) | 30 (46.15%) | |
| **Posterior** | 12 (44.44%) | 15 (23.08%) | |
| **Anterior + posterior** | 3 (11.11%) | 20 (30.77%) | |

**Table 2** The inter-reader and intra-reader reproducibility for DWI parameters

| parameters | ICC (95% CI) | |
|---|---|---|
| | inter-reader | intra-reader |
| **Standard DWI parameters** | | |
| ADC mean ($\times 10^{-3}$ mm$^2$/s) | 0.839 (0.721–0.906) | 0.978 (0.954–0.990) |
| eADC mean | 0.980 (0.958–0.991) | 0.975 (0.945–0.988) |
| **DKI parameters** | | |
| MD mean ($\times 10^{-3}$ mm$^2$/s) | 0.927 (0.851–0.965) | 0.917 (0.833–0.960) |
| MK mean | 0.979 (0.956–0.990) | 0.986 (0.972–0.994) |
| **IVIM parameters** | | |
| f mean (%) | 0.914 (0.824–0.958) | 0.904 (0.809–0.953) |
| D mean ($\times 10^{-3}$ mm$^2$/s) | 0.968 (0.935–0.985)) | 0.976 (0.951–0.989)) |
| D* mean ($\times 10^{-3}$ mm$^2$/s) | 0.972 (0.942–0.987) | 0.915 (0.828–0.958) |

in patients with PAS disorders (all $p < 0.05$) (Fig. 2, Table 3, supplement 1). At multivariate analysis, D mean (OR:2.45, 95% CI, 1.37–4.4) and D max (OR:0.45, 95% CI, 0.25–0.82) were identified as independent risk factors for PAS disorders. For discriminating PAS disorders, the AUCs of the above 2 parameters were 0.69 and 0.64

respectively while the AUC yielded 0.78 with the combined 2 parameters (Table 4). Significant differences were found in the AUCs between the combination of the 2 parameters and the separate 2 parameters (all $p < 0.05$) (Fig. 3).

Secondly, comparisons between accreta lesions in patients with PAS (AP) and whole placentas in patients with normal placentas (WP-normal) using volumetric analysis were performed. It demonstrated that MD mean, f mean, D mean and D* mean were significantly higher while ADC max, MK mean, MK max and D max were significantly lower in patients with PAS disorders (all $p < 0.05$) (Figs. 2 and 4, Table 3, supplement 1). At multivariate analysis, D mean (OR:4.12, 95% CI, 1.85–9.18) and D max (OR:0.15, 95% CI, 0.07–0.34) were identified as independent risk factors for PAS disorders. For discriminating PAS disorders, the AUCs of the above 2 parameters were 0.73 and 0.85 respectively while the AUC yielded 0.93 with the combined use of the 2 significant parameters (Table 4). Significant differences were found in the AUCs between the combination of the 2 parameters and D mean and D max (all $p < 0.05$) (Fig. 3).

## Discussion

Traditionally, most of the prior investigations [18–22, 24, 35, 36] measured DWI parameters from manually placed ROIs on one or several representative slices of the placenta, which may lead to interobserver variability in ROI selection. In addition, inappropriate ROI selection may not accurately reflect the physiological features of the placenta. Entire lesion volumetric analysis was adopted in our study to capture the parameters of the entire placenta and the accreta lesions in PAS disorders to eliminate sampling bias during data processing potentially. The intra- and interobserver agreements were excellent for all the parameters using the volumetric analysis. Therefore, the VOI-based estimation of DWI parameters was highly reproducible and repeatable.

Some studies have adopted IVIM to evaluate the placental function. Capuani's study demonstrated that ADC decreased with GA increase while f increased [24]. Jakab's study also demonstrated that f was moderately increasing during gestation [25]. However, Derwig's study reported that f did not change with GA [36], Sohlberg's and Kristi B's study reported that f decreased with GA [18, 22]. The inconsistency of the results from the above researches may arise from different ROI selections and different IVIM protocols. As for the influence of GA, parameters corrections were performed before the analysis to demonstrate the difference of the parameters between normal placentas and PAS disorders.

The placenta is a highly vascular organ containing both maternal and fetal vascular systems appropriate for IVIM
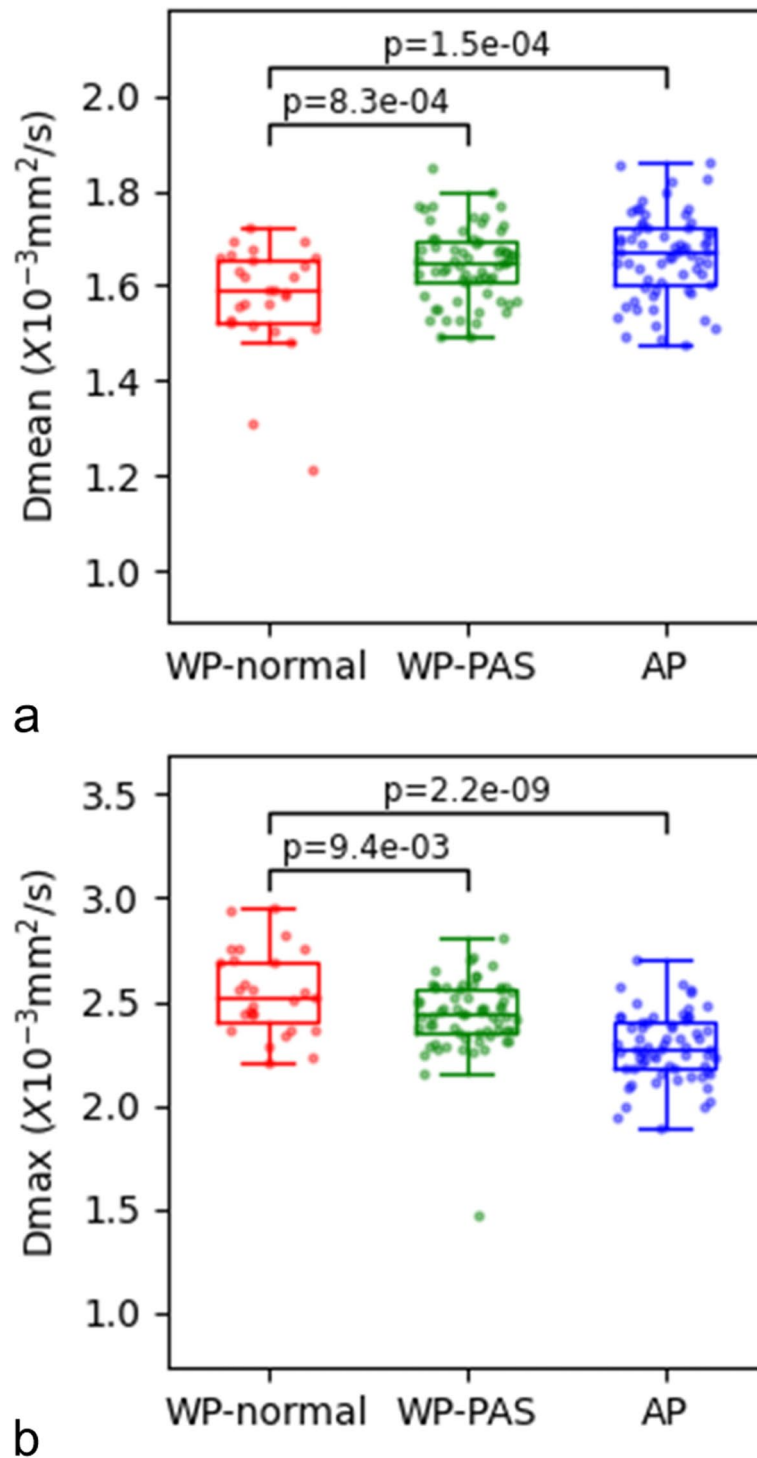
**Fig. 2** Box and whisker plots of D mean and D max for patients with normal placentas (Whole placenta-normal), patients with PAS disorders (Whole placenta-PAS) and accreta lesions in patients with PAS (AP)

analysis. The IVIM technique separates placental diffusion and perfusion based on the hypothesis that the diffusion-weighted signal in a voxel depends on a perfusion compartment described by $D^*$ and f and a diffusion compartment described by D. D is governed by random Brownian motion, representing the physical characteristic of the tissue, like cell size and membrane permeability.

Lu *et al. BMC Pregnancy and Childbirth*     (2022) 22:349

Page 7 of 12

**Table 3** Comparison of DWI parameters between patients with normal placenta and patients with PAS disorders ($n = 92$)

| parameters | Patients with PAS disorders | | Patients with normal placenta | P value | |
|---|---|---|---|---|---|
| | Whole placenta | Accreta lesions | Whole placenta | WP-normal vs WP-PAS | AP vs WP-normal |
| **Standard DWI parameters** | | | | | |
| ADC mean ($\times 10^{-3}$ mm$^2$/s) | 1.55 (0.08) | 1.56 (0.09) | 1.51 (0.12) | 0.076 | 0.180 |
| ADC min ($\times 10^{-3}$ mm$^2$/s) | 0.27 (0.39) | 0.51 (0.46) | 0.40 (0.32) | 0.061 | 0.265 |
| ADCmax ($\times 10^{-3}$ mm$^2$/s) | 2.43 (0.24) | 2.29 (0.24) | 2.49 (0.26) | 0.094 | 0.000 |
| eADC mean | 0.09 (0.01) | 0.09 (0.01) | 0.10 (0.02) | 0.099 | 0.155 |
| eADC min | 0.01 (0.01) | 0.02 (0.01) | 0.01 (0.01) | 0.394 | 0.055 |
| eADC max | 0.67 (0.32) | 0.46 (0.38) | 0.53 (0.29) | 0.096 | 0.522 |
| **DKI parameters** | | | | | |
| MD mean ($\times 10^{-3}$ mm$^2$/s) | 3.17 (0.39) | 3.15 (0.47) | 2.92 (0.26) | 0.005 | 0.005 |
| MD min ($\times 10^{-3}$ mm$^2$/s) | 0.26 (0.56) | 0.71 (0.84) | 0.44 (0.76) | 0.034 | 0.21 |
| MD max ($\times 10^{-3}$ mm$^2$/s) | 7.41 (0.92) | 7.14 (1.19) | 7.12 (0.56) | 0.000 | 0.29 |
| MK mean | 0.52(0.04) | 0.52 (0.04) | 0.53 (0.04) | 0.032 | 0.041 |
| MK min | 0 (0) | 0 (0) | 0 (0) | N/A | N/A |
| MK max | 1.68 (1.50) | 1.23 (0.75) | 1.87 (1.52) | 0.47 | 0.032 |
| **IVIM parameters** | | | | | |
| f mean (%) | 43.89 (4.65) | 43.18 (8.36) | 41.59 (4.50) | 0.010 | 0.041 |
| f min (%) | 0 (0) | 0 (0) | 0 (0) | N/A | N/A |
| f max (%) | 100 (0) | 100 (0) | 100 (0) | N/A | N/A |
| D mean ($\times 10^{-3}$ mm$^2$/s) | 1.65 (0.08) | 1.67 (0.12) | 1.59 (0.13) | 0.000 | 0.000 |
| D min ($\times 10^{-3}$ mm$^2$/s) | 0.31 (0.48) | 0.54 (0.53) | 0.37 (0.50) | 0.067 | 0.186 |
| D max ($\times 10^{-3}$ mm$^2$/s) | 2.44 (0.21) | 2.27 (0.22) | 2.52 (0.29) | 0.000 | 0.000 |
| D* mean ($\times 10^{-3}$ mm$^2$/s) | 36.0 (9.04) | 38.31 (11.18) | 30.34 (11.58) | 0.012 | 0.000 |
| D* min ($\times 10^{-3}$ mm$^2$/s) | 0 (0.02) | 0.29 (0.65) | 0 (0) | N/A | N/A |
| D* max ($\times 10^{-3}$ mm$^2$/s) | 100 (0) | 100 (0) | 100 (0) | N/A | N/A |

Our study showed that D mean and D max were independent risk factor for PAS disorders from comparisons between accreta lesions in patients with PAS (AP) and whole placentas in patients with normal placentas. The current hypothesis is supposed that the endometrium-myometrial interface defect caused by uterine scar leads to a failure of normal decidualization and allows extravillous trophoblastic infiltration and villous development in the deep myometrium [37]. Capuani's study identified that the normal placenta had higher cellularity and abundant cytoplasm, hindering water diffusion [24]. In this study, the D mean was significantly lower in normal placentas than in accreta lesions, supporting the previous hypothesis. D max was probably measured in areas with less water diffusion restriction. It had higher diagnostic accuracy than D mean in the accreta lesions, suggesting the noteworthy increased cellularity in certain areas in the accreta lesions. The diagnostic performance of the parameters from accreta lesions was better than parameters from the whole placenta. We further combined D

mean and D max for predicting PAS disorders, the diagnostic performance improved significantly with higher sensitivity, specificity, and accuracy of 83.08, 88.89, and 93.39%, respectively. It suggested the feasible combined use of the 2 DWI parameters in the quantitative evaluation and prediction of PAS disorders.

In the placenta, f represents the moving blood volume fraction compared with the total voxel volume and D* represents the blood movement in the intervillous spaces and the fetal capillaries [26]. In patients with PAS disorders, Uterine scars from previous CDs caused the local decidual deficit and the increasing number of partially or non-remodeled spiral arteries with abnormal EVT invasion into radial and arcuate arteries deep within the myometrium. It resulted in a hypervascular placental bed and massive blood loss when the invasive placenta detached [37, 38]. So the perfusion fraction increased in the accreta lesions and finally involved the whole placenta in patients with PAS disorders. Maternal blood flows slowly through the large pools of IVS, bathing the fetal villi and

Lu *et al. BMC Pregnancy and Childbirth*    (2022) 22:349

Page 8 of 12

**Table 4** Diagnostic value of DWI parameters in differentiating PAS disorders

| group | AUC(95%CI) | Optimal cutoff value | Youden index | sensitivity | specificity | +LR | -LR |
|---|---|---|---|---|---|---|---|
| WP-normal vs WP-PAS | | | | | | | |
| f mean(%) | 0.67 (0.56, 0.79) | 44 | 0.36 | 50.77% | 85.19% | 3.43 | 0.58 |
| D mean($\cdot 10^{-3}\,mm^2/s$) | 0.69 (0.58, 0.80) | 1.61 | 0.31 | 75.38% | 55.56% | 1.70 | 0.44 |
| D max($\cdot 10^{-3}\,mm^2/s$) | 0.64 (0.52, 0.76) | 1.75 | 0.29 | 95.38% | 33.33% | 1.43 | 0.14 |
| D* mean($\cdot 10^{-3}\,mm^2/s$) | 0.68 (0.57, 0.79) | 27.29 | 0.34 | 96.92% | 37.04% | 1.54 | 0.08 |
| MD mean($\times 10^{-3}\,mm^2/s$) | 0.68 (0.57,0.79) | 3.11 | 0.37 | 55.38% | 81.48% | 2.99 | 0.55 |
| MD min($\times 10^{-3}\,mm^2/s$) | 0.63 (0.51, 0.75) | 0.50 | 0.24 | 83.08% | 40.74% | 1.40 | 0.42 |
| MD max($\times 10^{-3}\,mm^2/s$) | 0.71 (0.60, 0.82) | 7.22 | 0.49 | 63.08% | 77.78% | 2.84 | 0.48 |
| Mkmean | 0.63 (0.51, 0.75) | 0.64 | 0.28 | 53.85% | 74.07% | 2.08 | 0.62 |
| Combined (D mean and D max) | 0.78 (0.68, 0.87) | 0.46 | 0.48 | 81.54% | 66.67% | 2.45 | 0.28 |
| AP vs WP-normal | | | | | | | |
| ADC max($\cdot 10^{-3}\,mm^2/s$) | 0.83 (0.75, 0.91) | 2.55 | 0.57 | 83.08% | 74.07% | 3.20 | 0.23 |
| f mean(%) | 0.62 (0.50 0.74) | 44 | 0.34 | 49.23% | 85.19% | 3.32 | 0.60 |
| D mean($\cdot 10^{-3}\,mm^2/s$) | 0.73 (0.63, 0.84) | 1.67 | 0.38 | 52.31% | 85.19% | 3.53 | 0.56 |
| D max($\cdot 10^{-3}\,mm^2/s$) | 0.85 (0.77, 0.93) | 2.41 | 0.60 | 86.15% | 74.07% | 3.32 | 0.19 |
| D* mean($\cdot 10^{-3}\,mm^2/s$) | 0.75 (0.65, 0.85) | 30.38 | 0.41 | 89.23% | 51.85% | 1.85 | 0.21 |
| MD mean($\times 10^{-3}\,mm^2/s$) | 0.68 (0.57, 0.79) | 3.12 | 0.37 | 55.38% | 81.485 | 2.99 | 0.55 |
| Mkmean | 0.63 (0.51, 0.75) | 0.64 | 0.26 | 52.31% | 74.07% | 2.02 | 0.64 |
| Mkmax | 0.64 (0.52, 0.76) | 1.52 | 0.30 | 75.38% | 55.56% | 1.70 | 0.44 |
| Combined (D mean and D max) | 0.93 (0.89, 0.98) | 0.46 | 0.72 | 83.08% | 88.89% | 7.48 | 0.19 |

enabling oxygen exchange between mothers and fetuses. The elevated D* mean values reflected the increased blood movement in the IVS and the fetal capillaries in the accreta lesions.

DKI has been increasingly implemented for providing more precise information on tissue cellularity and heterogeneity than conventional DWI. Because the former can quantify the non-Gaussian behavior of water diffusion, which is believed to reveal more genuine water molecular movement and distribution in biological tissues. MD is a corrected ADC value for the non-Gaussian diffusion and a diffusion-related coefficient. MD is correlated with tissue cellularity, showing a similar change to D in this study as MD mean values are significantly higher in accreta lesions. MK from DKI reflects the complexity or heterogeneity of the tissue. Thus the more significantly higher MK mean and MK max values represent more heterogeneous and irregular tissue components in normal placentas.

This study took the lead in combining two promising functional DWI models, DKI, and IVIM with conventional DWI models to characterize placental heterogeneity, cellularity, and microvascular perfusion at the same time and to distinguish PAS disorders. In this study, the accreta lesions were hyperperfused with

increased blood movement in the IVS and the fetal capillaries but with deceased cellularity and heterogeneity compared with normal placentas. These changes were prominent enough to involve the whole placenta but were more profound in the accreta lesions.

This study had some limitations. First, this study is retrospective with a small sample size, with the selection bias inevitable. Second, It was impossible to obtain breath-hold imaging from pregnant women, so the free-breathing protocol in this study was utilized. The good reproducibility of results confirmed the reliability of the measurements. Third, this study utilized 1600 s/mm² as the maximum b value, which is smaller than the recommended 2000 s/mm² for the rectal, renal, and hepatic lesions [29, 30, 39]. In this study, 11 b values ranging 0–1600 s/mm² in 3 orthogonal directions were adopted in the DKI sequence. It was feasible to use this DKI model in placental imaging because the DKI protocol in this study showed satisfactory overall imaging quality to the perfect intra- and inter-observer agreements.

In conclusion, placental function in PAS disorders changed miscellaneously, involving diffusion, perfusion, and heterogeneity of the placenta. Abnormal decidualization and subsequent villous infiltration in the
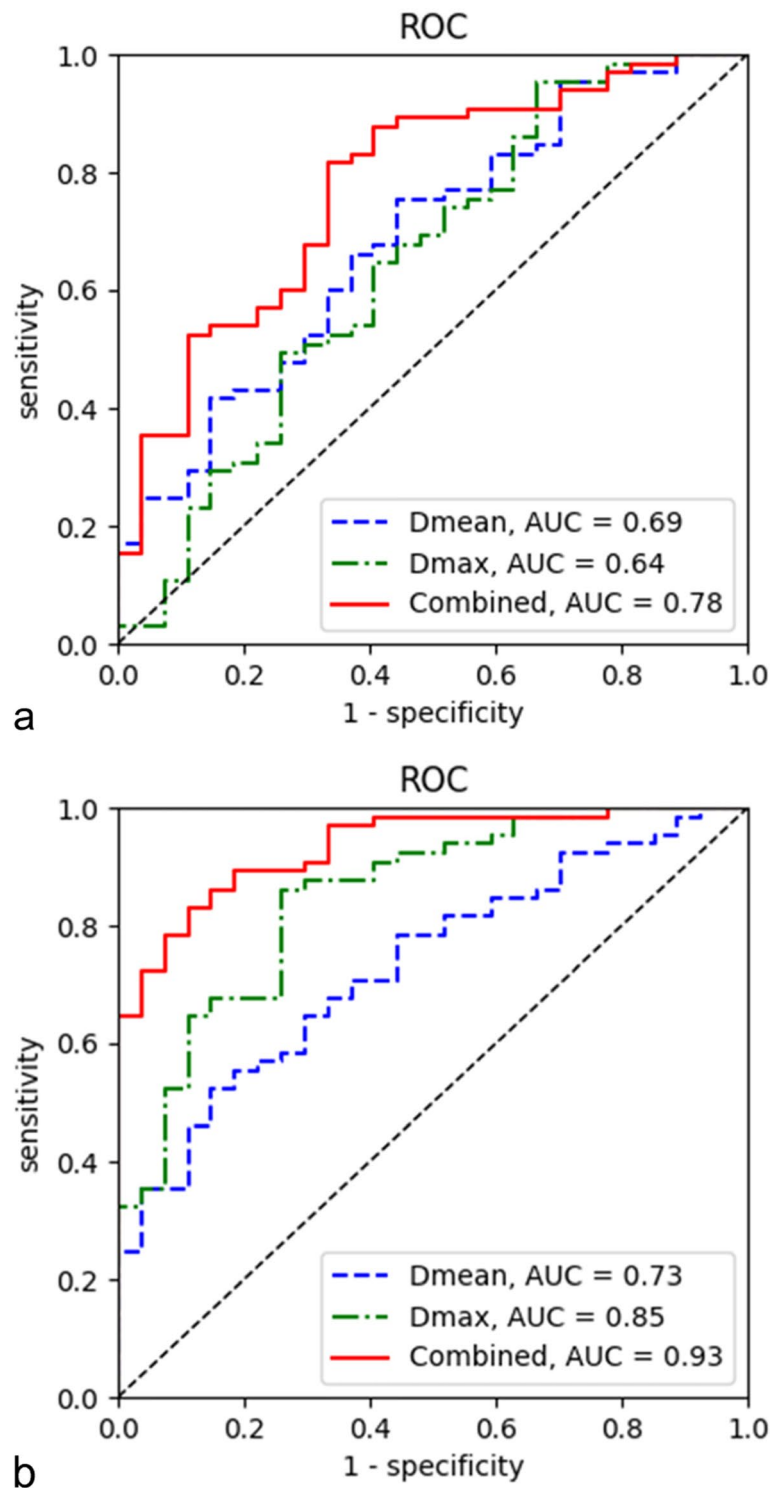
**Fig. 3** ROC (Receiver operating characteristics) curves for predicting PAS disorders based on parameters from different DWI (diffusion weighted imaging) models. **a** parameters from whole placenta comparisons, **b** parameters from accreta lesions vs normal placentas
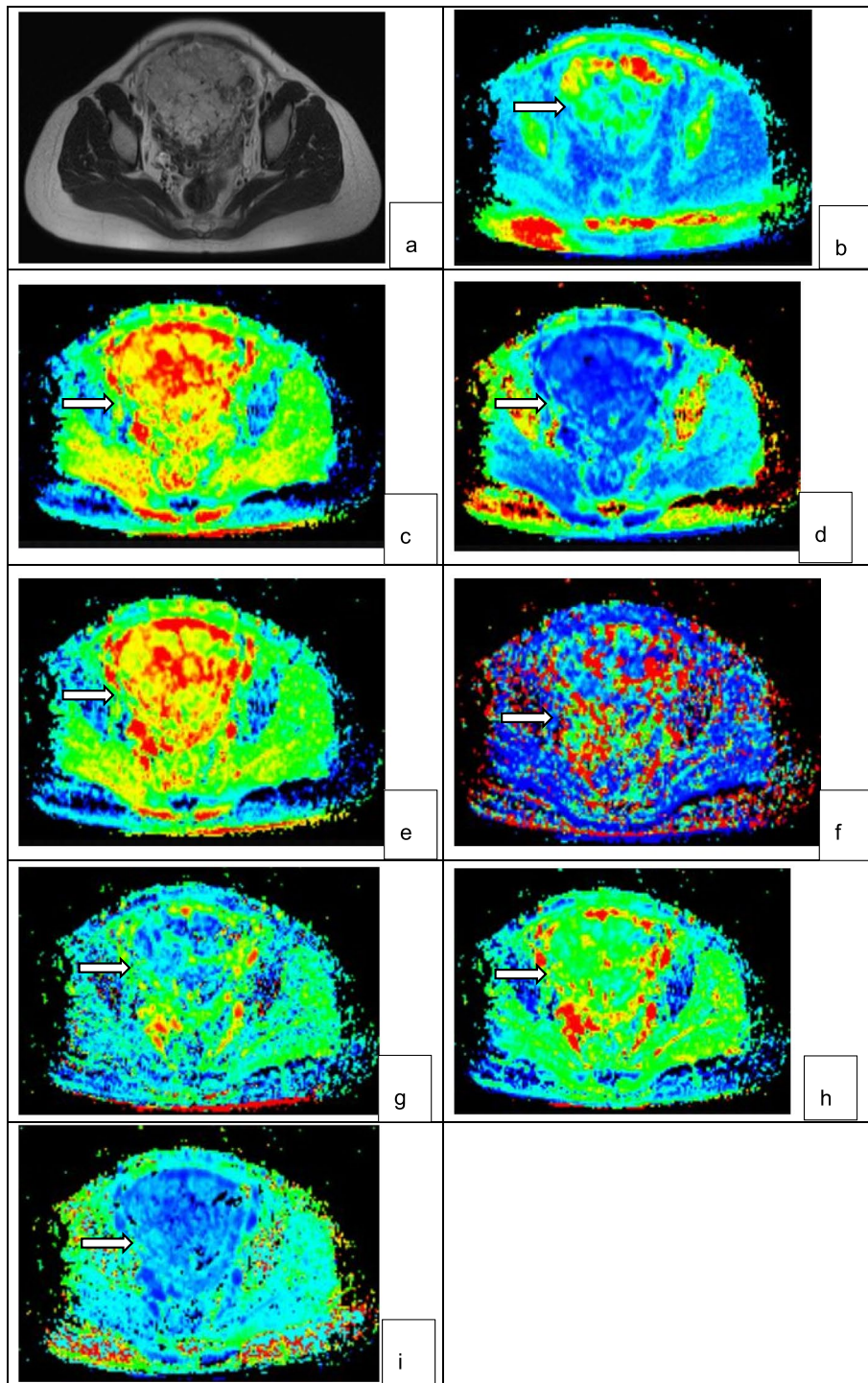
Lu *et al. BMC Pregnancy and Childbirth*    (2022) 22:349

Page 10 of 12



**Fig. 4** PAS disorders in a 33-year-old woman with prior cesarean delivery and placenta previa. (**a**)T2WI(T2 weighted imaging) showed abnormal vascularization of placental bed and abnormal intraplacental vascularity. The accreta lesion was generally iso- to hyperintense on DWI (**b**), heterogeneously hyperintense on ADC map (**c**) and hyperintense on eADC map (**d**) (white arrow). On IVIM(intravoxel incoherent motion) images, the lesions appeared heterogeneously hyperintense on D map (**e**), heterogeneous on D* map (**f**) and hypo- to isointense with some areas of hyperintense on f map (**g**) (white arrow). On DKI (diffusion kurtosis imaging) images, the lesions appeared iso- to hyperintense on MD map (**h**) and hypointense on MK map (**i**) (white arrow)

Lu *et al. BMC Pregnancy and Childbirth* (2022) 22:349

Page 11 of 12

myometrium resulted in the deceased cellularity and heterogeneity in the accreta lesions in adjunction with the increased relative amount of blood flowing through the vascular bed. Therefore, it is worthwhile and necessary to combine different DWI parameters in the comprehensive evaluation and accurate diagnosis of PAS disorders. Secondly, PAS disorders can be differentiated with the combined use of D mean and D max.

## Abbreviations

MRI: Magnetic resonance imaging; PAS: Placenta accreta spectrum; DWI: Diffusion weighted imaging; IVIM: Intravoxel incoherent motion; DKI: Diffusion kurtosis imaging; ADC: Apparent diffusion coefficient; eADC: Exponential apparent diffusion coefficient; MK: Mean kurtosis; MD: Mean diffusion coefficient; ROC: Receiver operating characteristics; WP-normal: Whole placentas in patients with normal placenta; WP-PAS: Whole placentas in patients with PAS; AP: Accreta lesions in patients with PAS; US: Ultrasonography; SAR: Society of Abdominal Radiology; ESUR: European Society of Urogenital Radiology; ROI: Region of interest; GA: Gestational age; CD: Cesarean delivery; ME: Monoexponential.

## Supplementary Information

The online version contains supplementary material available at https://doi.org/10.1186/s12884-022-04644-9.

**Additional file 1.** Supplementary Figure Box and whisker plots of ADC (ADC mean, ADC min, and ADC max), eADC (eADC mean, eADC min, and eADC max), MD (MD mean, MD min, and MD max), MK (MK mean and MK max), D (D min), D* (D* mean), and f (f mean) for patients with normal placentas (Whole placenta-normal), patients with PAS disorders (Whole placenta-PAS) and accreta lesions in patients with PAS (AP).

## Availability of data and materials
The datasets generated during and analyzed during the current study are not publicly available due to PACS system regulated by Sichuan Provincial People's Hospital, but are available from the corresponding author on reasonable request.

## Declarations

### Ethics approval and consent to participate
Written informed consent was obtained from each of the patient. The ethical review aboard of Sichuan Provincial People's Hospital approved the study and informed consent was obtained from each woman participating in the study. All methods were performed in accordance with the relevant guidelines and regulations.

### Consent for publication
Written consent for the publication of the clinical details of participants was obtained from each of the patient.

### Competing interests
The authors declare that they have no competing interest Funding.

### Author details
[1]Department of Radiology, Sichuan Academy of Medical Sciences & Sichuan Provincial People's Hospital, 32 West Second Section, First Ring Road, Chengdu 610072, China. [2]Siemens Healthineer, No.278, Zhouzhu Road, Pudong New Area District, Shanghai 201318, China. [3]School of Mechanical and Electrical Engineering, University of Electronic Science and Technology of China, 2006 Xiyuan Avenue, West Hi-tech Zone, Chengdu 611731, China.

### References

1. Jauniaux E, Ayres-de-Campos D. FIGO placenta Accreta diagnosis and management expert consensus Panel.FIGO consensus guidelines on placenta accreta spectrum disorders: introduction. Int J Gynaecol Obstet. 2018;140:261–4.
2. Jauniaux E, Chantraine F, Silver RM, et al. FIGO placenta Accreta diagnosis and management expert consensus Panel.FIGO consensus guidelines on placenta accreta spectrum disorders : epidemiology. Int J Gynaecol Obstet. 2018;140:265–73.
3. Miller DA, Chollet JA, Goodwin TM. Clinical risk factors for placenta previa placenta accreta. Am J Obstet Gynecol. 1997;177:210–4.
4. Wu S, Kocherginsky M, Hibbard J. U, abnormal placentation: twenty-year analysis. Am J Obstet Gynecol. 2005;192:1458–61.
5. Silver RM, Landon MB, Rouse DJ, et al. Maternal morbidity associated with multiple repeat cesarean deliveries. Obstet Gynecol. 2006;107:1226–32.
6. Shamshirsaz AA, Fox KA, Salmanian B, et al. Maternal morbidity in patients with morbidly adherent placenta treated with and without a standardized multidisciplinary approach. Am J Obstet Gynecol. 2015;212:218.e1–9.
7. Al-Khan A, Gupta V, Illsley NP, et al. Maternal and fetal outcomes in placenta accreta after institution of team-managed care. Reprod Sci. 2014;21:761.
8. Seoud MA, Nasr R, Berjawi GA, et al. Placenta accreta: elective versus emergent delivery as a major predictor of blood loss. J Neonatal Perinatal Med. 2017;10:9–15.
9. Camuzcuoglu A, Vural M, Hilali NG, et al. Surgical management of 58 patients with placenta praevia percreta. Wien Klin Wochenschr. 2016;128:360–6.
10. Norris BL, Everaert W, Posma E, et al. The urologist's role in multidisciplinary management of placenta percreta. BJU Int. 2016;117:961–5.
11. D'Antonio F, Iacovella C, Palacios-Jaraquemada J, et al. Prenatal identification of invasive placentation using magnetic resonance imaging: systematic review and meta-analysis. Ultrasound Obstet Gynecol. 2014;44:8–16.
12. Finazzo F, D'antonio F, Masselli G, et al. Interobserver agreement in MRI assessment of severity of placenta accreta spectrum disorders. Ultrasound Obstet Gynecol. 2020;55:467–73.
13. Rosenkrantz AB, Padhani AR, Chenevert TL, et al. Body diffusion kurtosis imaging: basic principles, applications, and considerations for clinical practice. J Magn Reson Imaging. 2015;42:1190–202.
14. Jensen JH, Helpern JA, Ramani A, et al. Diffusional kurtosis imaging: the quantification of non-gaussian water diffusion by means of magnetic resonance imaging. Magn Reson Med. 2005;53:1432–40.
15. Jensen JH, Helpern JA. MRI quantification of non-Gaussian water diffusion by kurtosis analysis. NMR Biomedicine. 2010;23:698–710.
16. Le Bihan D. Intravoxel incoherent motion imaging using steady-state free precession. Magn Reson Med. 1988;7:346–51.
17. Le Bihan D. Molecular diffusion, tissue microdynamics and microstructure. NMR Biomed. 1995;8:375–86.
18. Kristi BA, Ditte NH, Caroline H, et al. Placental diffusion-weighted MRI in normal pregnancies and those complicated by placental dysfunction due to vascular malperfusion. Placenta. 2020;91:52–8.

19.  Lu T, Pu H, Li K, et al. Can introvoxel incoherent motion MRI be used to differentiate patients with placenta accreta spectrum disorders? BMC Pregnancy Childbirth. 2019;19:531.

20.  Lu T, Song B, Pu H, et al. Prognosticators of intravoxel incoherent motion (IVIM) MRI for adverse maternal and neonatal clinical outcomes in patients with placenta accreta spectrum disorders. Transl Androl Urol. 2020;9(2):258–26.

21.  Lu T, Pu H, Cui W, et al. Use of intravoxel incoherent motion MR imaging to assess placental perfusion in patients with placental adhesion disorder on their third trimester. Clin Imaging. 2019;56:135–9.

22.  Sohlberg S, Mulic-Lutvica A, Lindgren P, et al. Placental perfusion in normal pregnancy and early and late preeclampsia: a magnetic resonance imaging study. Placenta. 2014;35:202–6.

23.  Moore RJ, Strachan BK, Tyler DJ, et al. In utero perfusion fraction maps in normal and growth restricted pregnancy measured using IVIM echoplanar MRI. Placenta. 2000;21(7):726–3.

24.  Capuani S, Guerreri M, Antonelli A, et al. Diffusion and perfusion quantified by Magnetic Resonance Imaging are markers of human placenta development in normal pregnancy. Placenta. 2017;58:33–9.

25.  Jakab A, Tuura RL, Kottke R, et al. Microvascular perfusion of the placenta,developing fetal liver, and lungs assessed with intravoxel incoherent motionimaging. J Magn Reson Imaging. 2018;48:214–25.

26.  Moore RJ, Issa B, Tokarczuk R, et al. In vivo intravoxel incoherent motion measurements in the human placenta using echo-planar imaging at 0.5T. Magn Reson Med. 2000;43(3):295–302.

27.  Yang M, Yan Y, Wang H. IMAge/enGINE: a freely available software for rapid computation of highdimensional quantification. Quant Imaging Med Surg. 2018. https://doi.org/10.21037/qims.2018.12.03.

28.  Xiao Z, Zhong Y, Tang Z, et al. Standard diffusion-weighted, diffusion kurtosis and intravoxel incoherent motion MR imaging of sinonasal malignancies: correlations with Ki-67 proliferation status. Eur Radiol. 2018;28:2923–33.

29.  Cui Y, Yang X, Du X, et al. Whole-tumour diffusion kurtosis MR imaging histogram analysis of rectal adenocarcinoma: correlation with clinical pathologic prognostic factors. Eur Radiol. 2018;28:1485–94.

30.  Ding Y, Tan Q, Mao W, et al. Differentiating between malignant and benign renal tumors: do IVIM and diffusion kurtosis imaging perform better than DWI? Eur Radiol. 2019;29:6930–9.

31.  Wan Q, Deng Y, Lei Q, et al. Differentiating between malignant and benign solid solitary pulmonary lesions: are intravoxel incoherent motion and diffusion kurtosis imaging superior to conventional diffusion-weighted imaging? Eur Radiol. 2019;29:1607–15.

32.  Jauniaux E, Ayres-de-Campos D, Langhoff-Roos J, et al. FIGO placenta Accreta diagnosis and management expert consensus panel. FIGO classification for the clinical diagnosis of placenta accreta spectrum disorders. Int J Gynaecol Obstet. 2019;146(1):20–4.

33.  Sun H, Qu H, Chen L, et al. Identification of suspicious invasive placentation based on clinical MRI data using textural features and automated machine learning. Eur Radiol. 2019;29:6152–62.

34.  Pedregosa F, Varoquaux G, Gramfort A, et al. Scikit-learn: machine learning in Python. J Mach Learn Res. 2011;12:2825–30.

35.  Bao Y, Pang Y, Sun Z, et al. Functional diagnosis of placenta accreta by intravoxel incoherent motion model diffusion-weighted imaging. Eur Radiol. 2020;31(2):740–74.

36.  Derwig I, Lythgoe DJ, Barker GJ, et al. Association of placental perfusion, as assessed by magnetic resonance imaging and uterine artery doppler ultrasound, and its relationship to pregnancy outcome. Placenta. 2013;34:885–91.

37.  Kim K-R, Jun S-Y, Kim J-Y, Ro J-Y. Implantation site intermediate trophoblasts in placenta Cretas. Mod Pathol. 2004;17:1483–90.

38.  Khong TY, Robertson WB. Placenta creta and placenta praevia creta. Placenta. 1987;8:399–409.

39.  Cao L, Chen J, Duan T, et al. Diffusion kurtosis imaging (DKI) of hepatocellular carcinoma: correlation with microvascular invasion and histologic grade. Quant Imaging Med Surg. 2019;9(4):590-602.

## Publisher's Note